Direct measurements of xanthine in 2000-fold diluted xanthinuric urine with a nanoporous carbon fiber sensor

Mehjabin Kathiwala, Andrews Obeng Affum, Jason Perry and Anna Brajter-Toth*

Received 23rd November 2007, Accepted 21st February 2008
First published as an Advance Article on the web 12th March 2008
DOI: 10.1039/b718125f

High selectivity and sensitivity is reported in the measurements of xanthine in urine by fast scan cyclic voltammetry (FSV) with a nanostructured carbon fiber sensor of 3.5 ± 0.4 μm radius. Fabrication of the sensors for the measurements is described. Fabrication of the nanostructure at the carbon fiber sensor surface exposes surface pores. SEM images confirm the formation of the nanostructure. The results indicate that the nanostructure improves the sensitivity and limit of detection (LOD) in the measurements of xanthine and uric acid. The sensors allow rapid direct measurements of xanthine in 2000-fold diluted xanthinuric urine and of uric acid in 2000-fold diluted normal urine. The sensitivity and the LOD of xanthine is 0.40 ± 0.02 nA μM^{-1} (0.995) and 1 μM, respectively, and 0.99 ± 0.01 nA μM^{-1} (0.998) and 500 nM for uric acid. The concentration of xanthine in 2000-fold diluted xanthinuric urine is 1.6 ± 0.2 μM from FSV and from HPLC. The concentration of xanthine and uric acid in urine can be determined by pre- or post-calibration of the sensor in buffer or by the method of standard addition.

Introduction

Purines are key cellular building blocks and their synthesis and salvage is carefully regulated, as illustrated in Fig. 1.[1] Disruptions of the purine cycle by, for example, hypoxic stress, lead to the accumulation of purines in the brain,[2] heart and kidneys,[3,4] and can lead to disease.[5] Diseases such as diabetes, arthritis, gout, and high blood pressure have been linked to high levels of uric acid in blood and urine.[5,6] Screening for abnormal purine profiles, which requires measurements of uric acid and xanthine in biological fluids, has been recommended in the diagnosis of inborn metabolic disorders and of diseases.[7,8] Xanthine, which is the metabolic precursor of uric acid, is the first indicator of an abnormal purine profile, and can serve as a marker of acute hypoxic stress.[9] Hypoxanthine, the precursor of xanthine, can be recycled *via* a salvage pathway (Fig. 1). Concentrations of uric acid in the normal human urine range from 2 to 8 mM;[10] xanthine between 41 and 161 μM;[11] and hypoxanthine from 22 to 92 μM.[11]

HPLC and capillary electrophoresis (CE) with UV detection have been used in xanthine measurements in blood serum,[12,13] urine[14] and saliva,[15] after separation from uric acid and quantification at different wavelengths.[16] CE with UV detection has the limit of detection (LOD) of 0.56 μM for xanthine;[13] the LOD of HPLC/UV is 0.5 μM.[11] In the electrochemical measurements the LOD of xanthine in the nanomolar,[17] submicromolar[18] and micromolar[19] ranges have been reported.

Electrochemical sensors have major advantages in biological analysis: of speed of measurements, simple portable instrumentation, inexpensive and readily available materials, and ease of miniaturization. Nanomaterials-based electrochemical sensor technology is particularly promising for biological analysis.[20,21] The LODs for xanthine that have been reported indicate that sensitive electrochemical sensors can be fabricated for practical clinical analysis.

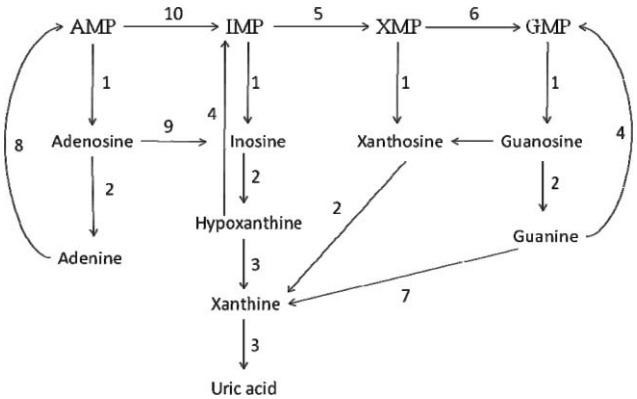

Fig. 1 Metabolic pathway of purines in humans: 1 = 5′-nucleotidase, 2 = purine nucleoside phosphorylase, 3 = xanthine oxidase, 4 = hypoxanthine-guanine phosphoribosyl transferase, 5 = inosine 5′-monophosphate dehydrogenase, 6 = guanine monophosphate synthetase, 7 = guanine deaminase, 8 = adenine phosphoribosyl transferase, 9 = adenosine deaminase and 10 = AMP deaminase. AMP = adenosine monophosphate, IMP = inosine monophosphate, XMP = xanthosine monophosphate and GMP = guanosine monophosphate. (Adapted from ref. 13.)

Since the sample volume is generally not an issue, a conventional graphite electrode, with a diameter in the millimeter range, can be used in urine analysis. Previous electrochemical measurements of xanthine, which achieved limits of detection in the nanomolar range, were performed with a conventional size rough pyrolytic graphite (RPG) electrode by square wave

University of Florida, Department of Chemistry, Gainesville, FL 32611-7200, USA. E-mail: atoth@chem.ufl.edu

voltammetry.[17] However, because of the problems with the reproducibility of the RPG surface in this method, the reproducibility of the measurements was low. Determinations of xanthine with a carbon fiber sensor have been reported, but the sensitivity and resolution were lower than required in biological measurements because of the unstable background current in the reported method.[22]

Carbon fiber sensors developed by Brajter-Toth *et al.*[20] have been shown to have high sensitivity in the measurements of small metabolites by fast scan voltammetry (FSV).[23,24] The high sensitivity of the sensors is due to the high activity and stability of the nanostructured surface, and to the method of signal acquisition by FSV. A very large surface area is obtained by the method of fabrication of the nanostructure at the carbon fiber surface. At the nanostructured carbon fiber surface, charge transport is facilitated without restricting mass transport.

Measurements of uric acid with the nanostructured carbon fiber sensor by FSV, directly in 1000-fold diluted urine, have been reported.[25] The results demonstrated the advantages of the electrochemical sensor for direct, rapid screening of urine samples. Determinations of purine metabolites in urine, after higher (2000-fold) dilution of urine samples, were tested in this work. It was expected that in more dilute samples, better background subtraction, of a more stable background, would improve the signal-to-noise ratio and increase the sensitivity in the FSV measurements. Further, the method of measurements of xanthine and uric acid in highly diluted samples can be applied to cellular samples. Finally, the results indicate that the high dilution benefits the determinations of xanthine, because it facilitates rapid oxidation of xanthine in FSV.

Sensors with a reproducible surface structure, and dimensions, have been difficult to fabricate, which has resulted in a general requirement for frequent sensor calibration in biological measurements.[26,27] In this work, the reproducibility of sensor fabrication was improved, and sensor selection criteria were developed that were based on the measurement of sensor radius and activity, which allowed pooling of the data that were obtained with different sensors, and eliminated the need for frequent sensor calibration.

Determinations of xanthine in urine of a xanthinuric patient are reported. Xanthinuria is a rare autosomal disease that is marked by the deficiency of xanthine oxidase; it can also occur as a result of the treatment of gout and arthritis.[28,29] The condition elevates xanthine levels, with little or no uric acid being produced, while the concentration of hypoxanthine is between 6 and 50 μM[11] due to the up-regulation of the salvage pathway.[30] Degradation of guanine nucleotides to xanthine bypasses the hypoxanthine salvage pathway, and may explain the predominance of xanthine in xanthinuria.[30] In addition, direct measurements of uric acid in 2000-fold diluted normal urine are shown.

Experimental

Materials

All chemicals were obtained from Fisher (Pittsburgh, PA) and Sigma-Aldrich (St. Louis, MO). HPLC filters were from Millipore (Billerica, MA) and GE Osmonics Labstore (Minnetonka, MN). Solutions were prepared before each experiment. Sodium phosphate buffer, pH 7.4, was prepared with sodium phosphate monobasic monohydrate ($NaH_2PO_4 \cdot H_2O$) and sodium phosphate dibasic anhydrate (Na_2HPO_4). The pH was adjusted with 0.1 M NaOH or KOH (for HPLC) before the experiments. All determinations were performed at room temperature. The xanthinuric urine sample was a gift from Guy's Hospital, UK and normal urine was obtained from healthy volunteers. Urine samples were diluted with phosphate buffer, pH 7.4.

HPLC measurements

The HPLC system was comprised of a Hewlett Packard Series 1050 pulse-less pump (Avondale, PA) with a manual 20.0 μL injector loop and Spectra 100 detector (Spectra Physics, Irvine, CA). The chromatograms were acquired with PicoLog software (Pico Technology Ltd, St. Neots, UK) and were processed using Origin 6.0 (OriginLab Corporation, Northhampton, MA).

A Burdick & Jackson (Muskegon, MI) C-18 column, 4.6 × 250 × 5 mm, was maintained at room temperature and was conditioned with 1 : 1 methanol–water for 30 min, water for 1 h and a mobile phase of 20 mM potassium dihydrogen phosphate, pH 5.1 for 45 min.[31] The flow rate was 1.0 mL min^{-1}. The retention time of uric acid is 7.2 ± 0.1 min and of xanthine is 15.2 ± 0.2 min.

Electrochemical measurements

The instrumentation and the method of signal acquisition has been described previously.[25] Background current was recorded from −1.0 to 1.5 V, as shown in Fig. 2, by averaging 250 voltammograms in buffer, and was subtracted from 250 averaged voltammograms of the sample.[32] The average current of at least

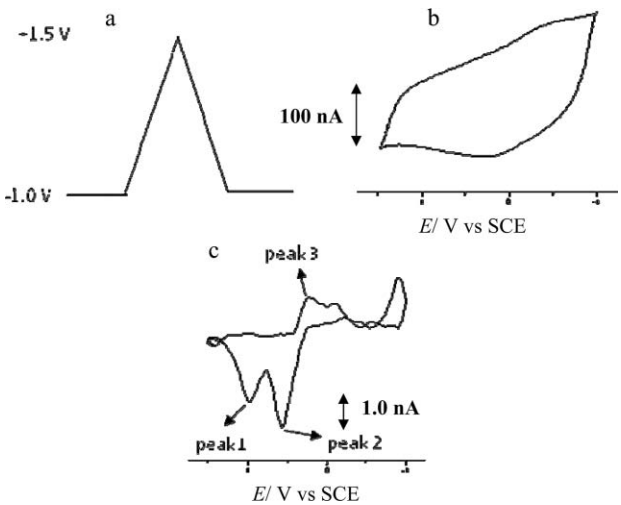

Fig. 2 Fast scan voltammetry of xanthine in buffer: (a) continuous applied potential waveform from −1.0 to +1.5 V *vs.* SCE; (b) large background current in buffer at 500 V s^{-1}; (c) background-subtracted voltammogram of 2.5 μM xanthine: the peak at 0.85 V (peak 1) represents xanthine oxidation and the peak at 0.5 V (peak 2) is the oxidation peak of uric acid generated from xanthine oxidation; the reduction peak of the uric acid oxidation product, the diimine, is at peak 3. 31 mM phosphate, pH 7.4; average of 250 scans; 500 V s^{-1}; carbon fiber sensor radius 3.5 μm.

3 determinations is reported. Xanthine current was measured at 0.85 V and of uric acid at 0.5 V *vs* SCE.

Electrodes

A polyacrylonitrile (PAN)-based carbon fiber (7.5 μm diameter; Textron Specialty Materials, Lowell, MA) was the working electrode material. The sensor fabrication procedure has been described in detail elsewhere.[25] The previous procedure was modified by touch-polishing of the sealed fiber on 600-grit SiC paper (Mark V Laboratory, East Granby, CT), on a polishing wheel (Ecomet I, Buehler Laboratory, Evanston, IL), and washing with doubly distilled water before the electrochemical measurements. Sensors that gave a response in 5 mM $K_3Fe(CN)_6$ in 0.5M KCl (pH 6.0) at 50 mV s^{-1}, corresponding to the theoretical diameter of the carbon fiber (7.5 μm), were used for analysis. A disk geometry was assumed and the diffusion coefficient of $Fe(CN)_6^{3-}$ is 7.7×10^{-6} cm^2 s^{-1}.[33] The capacitance of the sensor is higher if the resin packing surrounding the fiber contains voids and/or if there is an excess of the conducting epoxy, which is used to connect the carbon fiber to the copper wire.[34] This can be avoided during fabrication. A saturated calomel electrode (SCE) was the reference electrode (Fisher Scientific, Pittsburg, PA).

SEM imaging

SEM images were obtained using a Hitachi S4000 FE-SEM. The carbon fiber was coated along its length with nail varnish, to expose the disk surface. Carbon fibers insulated with the varnish were treated by the electrochemical oxidation and reduction in buffer, as described in the literature.[24] After the electrochemical treatment, before the SEM analysis, the fibers were dipped in doubly deionized water for cleaning. The cleaved fibers, which were coated with nail varnish, but were not electrochemically treated, were also imaged. To improve the quality of the SEM images, the fibers were sputtered with a thin Au/Pd film, using a Desk II Cold Sputter instrument (Denton Vacuum, LLC, Moorestown, NJ).

Analytical determinations

Sensitivity is reported as the average slope of the calibration plots for at least four concentrations and tree determinations at each concentration of at least six determinations (six electrodes). The limit of detection (LOD) is reported for a signal-to-noise ratio of 3 of peak-to-peak noise. Normal urine samples were obtained from six healthy individuals. Since xanthinuria is a rare disease, only one sample was available for analysis.

Standard addition

A 50 μL urine sample was diluted to 100 mL with 31 mM phosphate buffer, pH 7.4. Standard addition was performed for 2 or 4 μM final concentration in 10 mL. The solubility of xanthine is 130 mg L^{-1} or 8.5×10^{-4} M at pH 7.0.[35] Xanthine stock solutions (50 μM) were sonicated for at least 15–20 min.

Results and discussion

Background current and surface structure of the carbon fiber sensor

Carbon fibers have been used successfully for the past 20 years as materials for electrochemical sensors.[36] However, new materials are needed to improve the sensitivity and selectivity in biological analysis. Nanostructured electrochemical sensor materials have demonstrated advantages in biological analysis.[20,21]

Sensitive and stable nanostructured PAN-based carbon fiber electrochemical sensors have been fabricated by electrochemical methods.[20] Electrochemical oxidation, followed by reduction, between +1.5 and −1.0 V, by slow potential cycling in buffer, can expose and connect surface pores that are present in PAN fibers as a result of the manufacturing process,[37] and a stable surface nanostructure is obtained.

Eqn (1)–(5) summarize the reactions at the surface.[38–40] O_2-containing surface functional groups, formed at positive potentials [eqn (1)], can be reduced at negative potentials, with the evolution of CO_2.[40] CO_2, O_2, OH^- and H_2 are produced at positive and negative potentials, respectively [eqn (2)–(5)]. The evolution of CO_2 and H_2 contributes to the formation of surface pores,[38] together with the intercalation and deintercalation of electrolyte and water.[40]

$$C_x + 2H_2O \rightarrow C_xO_2H_y + (4 - y)H^+ + (4 - y)e^- \quad (1)$$

where $x = 8$–12 and $y = 1$–2

$$C + 2H_2O \rightarrow CO_2 + 4H^+ + 4e^- \quad (2)$$

$$2H_2O \rightarrow O_2 + 4H^+ + 4e^- \quad (3)$$

$$2H_2O + O_2 + 4e^- \rightarrow 4OH^- \quad (4)$$

$$2H_2O + 2e^- \rightarrow 2OH^- + H_2 \quad (5)$$

SEM images were obtained to gain insight into the surface structure of PAN carbon fiber sensors. Formation of pores at the surface has been postulated previously from electrochemical measurements, from the increase in sensor surface area after the electrochemical oxidation and reduction of the surface, as described above. The experimental difficulties of imaging surfaces of *ca.* 7 μm diameter, of fibers supported by epoxy, in plastic structures of much larger diameter, were overcome here by insulating the sides of the fiber with a thin coating of nail varnish, which unambiguously exposed the conducting fiber surface. When the SEM images were obtained, the thin coating of the insulator allowed easy location in the insulating layer of the conductive disk surface.

Fig. 3 shows the SEM images of the surfaces of the cleaved (electrochemically untreated), and of the electrochemically treated PAN carbon fibers. The structure of the cleaved surface shows visible defects and pores, in agreement with previous reports.[41] The cleaved surface is rough and has a step-like (ladder-like) appearance, which has been reported.[42] The cleaved PAN fiber surface is highly irregular because of the nanofeatures at the surface; however, no major pores are visible on the surface. Along the entire length of the fiber, along the fiber edge, there are transverse ridges, but there are few apparent

gaps between these ridges. After the electrochemical treatment, the most prominent change is the appearance of the exposed pores on the surface (Fig. 3). [It is important to note the lower magnification in Fig. 3(b) which clearly shows the pores.] An additional important change in the surface structure after the electrochemical treatment is the appearance of the cracks along the transverse ridges, along the edge of the fiber, and nodules visible in some regions of the surface.

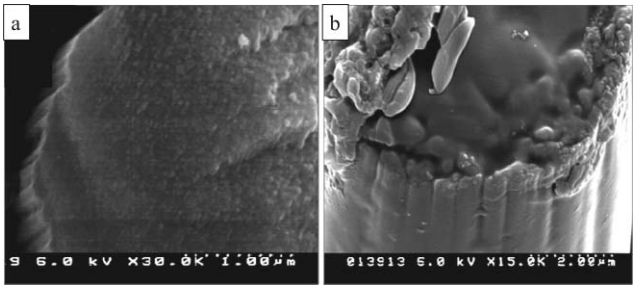

Fig. 3 SEM images of the carbon fiber before (a) and after (b) electrochemical treatment. The increase in the width of the edge dimensions from 140 to 200 nm and the appearance of pores can be seen in (b).

Charging of the fiber surface is observed in Fig. 3(a), consistent with the relatively high porosity of PAN fibers.[43] After the electrochemical oxidation and reduction, salt deposits are visible on the surface, from buffer electrolyte which is not completely washed off after the electrochemical treatment of the surface before SEM imaging. SEM shows that the pores on the surface are better defined, in agreement with higher background current after the electrochemical oxidation and reduction of the surface [Fig. 4(a)].

Fig. 4(a) illustrates the background current of the nanostructured PAN sensor, fabricated by the procedure described above. Of interest is the magnitude of the background current at +1.5 V, which measures the extent of the over-oxidation of the surface.[20,44] A small current at +1.5 V, such as in Fig. 4(a), indicates a limited over-oxidation of the surface.[20] From mostly capacitive current at +0.75 V, the increase in surface area by the nanostructure can be determined.[45]

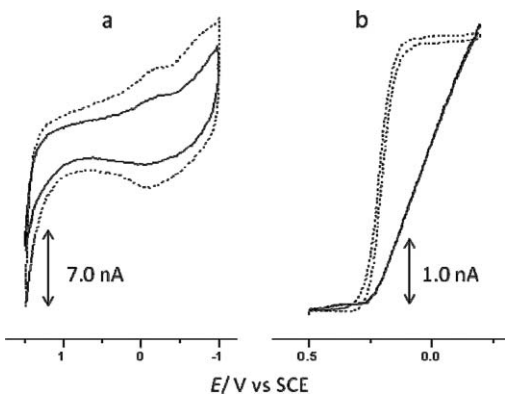

Fig. 4 Characterization of the sensor by slow scan voltammetry before (solid line) and after (dotted line) electrochemical treatment: (a) background current at 10 V s^{-1} in buffer, 50 cycles averaged; (b) 5 mM $K_3Fe(CN)_6$ in 0.5 M KCl, pH 6.0, at 50 mV s^{-1}.

Voltammetry of ferricyanide

Steady-state response from slow scan voltammetry at 50 mV s^{-1} of 5 mM ferricyanide can be used to select sensors without major defects.[20,46] Fig. 4(b) (dotted line) represents a response of a sensor for which the geometric disk radius determined from the limiting current[46] is in good agreement with the manufacturers' value. The radius determined from the limiting current, greater than 3.5 ± 0.4 μm, the value provided by the manufacturer, likely reflects surface geometry other than the disk. The electrochemical activity of the sensors was confirmed from the slope of around 60 mV of the E *vs.* log $(i_L - i)/i$ plot,[46] which is the value expected for active sensors;[20] only active sensors were used in analysis. The increase in the sensor surface area, by the nanostructure, is not evident from slow scan voltammetry of ferricyanide. The diffusion-limited current in slow scan voltammetry at 50 mV s^{-1} cannot be used to diagnose the presence of scratches or pores of nanometer dimensions, smaller than the average diffusion length of 28 μm, which were identified by SEM [Fig. 3(b)]. The experiments with 5 mM ferricyanide at slow scan rates were conducted with the purpose of verifying the surface radius, and of identifying active sensors for the measurements.

Voltammetry of xanthine

The xanthine oxidation peak in FSV is half the height of the uric acid oxidation peak [Fig. 2(c)]. Uric acid forms in the electrochemical oxidation of xanthine [Fig. 2(c), peaks 1 and 2]. Uric acid has a lower oxidation potential than xanthine, and is oxidized at the potentials of xanthine oxidation in a fast, $2e^-$, $2H^+$ reaction.[47] The reduction peak of the uric acid oxidation product, the diimine [peak 3, Fig. 2(c)], is smaller than the uric acid oxidation peak because the diimine is easily hydrolyzed.[47]

The results of FSV are consistent with fast, $1e^-$ oxidation of xanthine[48,49] to xanthine radicals (**I**) (Scheme 1). Further oxidation of the radicals to uric acid, following H^+ loss, which can be slow, competes at high xanthine concentrations with the disproportionation of the radicals (Scheme 1).[50] Broadening of the xanthine oxidation peak at high concentrations of xanthine is a result of the chemical reactions which follow the FSV oxidation of xanthine.

The formation of xanthine radical intermediates, which decay by disproportionation to xanthine, has been proposed from EPR studies of xanthine oxidation with sulfate and hydroxyl radicals.[48,49] From these studies the distribution of xanthine oxidation products was found to be concentration dependent.[50] Scheme 1 parallels the pathways from pulse radiolysis.

The oxidation peak potential of xanthine of 0.83 ± 0.06 V (pH 7.4) *vs.* SCE in FSV is more positive than 0.62 V (*vs.* SCE) predicted at pH 7 from slow scan voltammetry[51] and $E^{0\prime} = 0.35$ V *vs.* SCE (pH 13) from pulse radiolysis and EPR measurements.[52] From slow scan voltammetry, the oxidation peak potential of 0.36 V *vs.* SCE is predicted at pH 12.[51] Xanthine pK_a values are 0.8, 7.44 and 11.12.[53] The positive peak shift in FSV in xanthine oxidation is due in part to the high iR drop in FSV.[54] The reaction pathway may also be different in FSV; the pathway is different at low xanthine concentrations, where the competing following chemical reactions do not interfere with the oxidation.

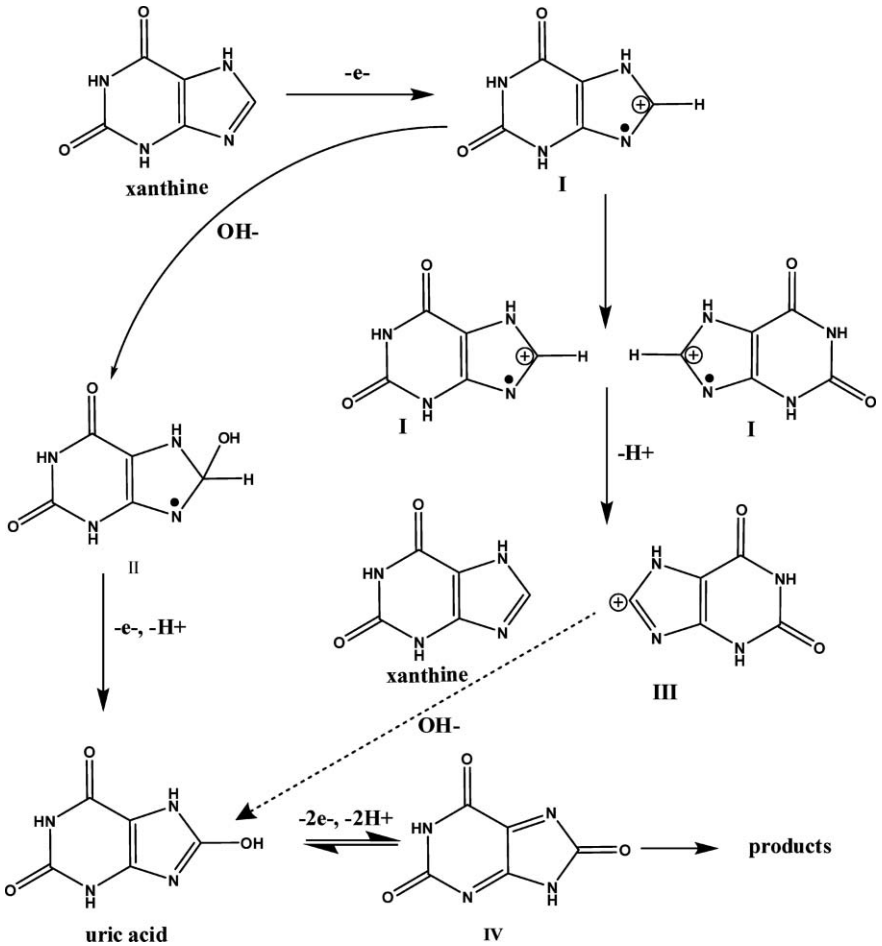

Scheme 1 Proposed electrochemical oxidation pathway of xanthine.

Sensitivity in fast scan voltammetry of xanthine

In the slow scan voltammetry of xanthine at 10 V s^{-1}, the LOD of 6 μM, and low resolution of xanthine and uric acid peaks, has been reported at a PAN carbon fiber sensor.[22] A stable background current at 0.83 ± 0.06 V, the potential of the xanthine oxidation peak, is needed for good S/N. The stable background is difficult to achieve during voltammetric measurements because the surface reactions such as the reactions above can change the surface structure of the sensor, which can change the background current. At positive potentials of xanthine oxidation the contribution of surface reactions to the background current is expected to increase. However, at +0.75 V at 500 V s^{-1} the background current that was measured was only 35 times higher than at 10 V s^{-1} [Fig. 2(b)] or lower than expected from the direct dependence of the charging (background) current on the scan rate. At 10 V s^{-1} the oxidation reactions of/at the sensor surface can contribute to the background current, but appear to be limited at 500 V s^{-1}, possibly due to slow kinetics. This and signal averaging can improve the S/N at 500 V s^{-1}.

In FSV at 500 V s^{-1}, the xanthine (10 μM) peak current is 3.2 ± 0.2 nA *vs.* the theoretical current of 3.6 × 10^{-2} nA, or, the observed peak current is 88 times higher than the calculated value for an irreversible reaction.[46] At 10 V s^{-1}, the xanthine oxidation peak current is 0.30 ± 0.02 nA (radius 3.6 μm), *ca.* 60 times higher than the theoretical current. Xanthine and uric acid oxidation peaks are well-resolved in FSV at 500 V s^{-1} [Fig. 2(c)]. Similarly, at 500 V s^{-1}, the peak current of uric acid is 100 times greater than the theoretical current. The nanostructure of the sensor, with the large surface area, of the low volume surface pores, and the FSV method of signal acquisition, which limits contributions to the response of slower reactions, such as the oxidation reactions at/of the surface, are responsible for the improved sensitivity, LOD and the resolution of the measurements. The higher sensitivity at 500 V s^{-1} verifies that the pores are exposed and that the larger surface area is available to the analyte as the diffusion layer shrinks. The diffusion layer thickness at 500 V s^{-1} of approx. 230 nm approaches the diameter of the pores visible in the SEM images [Fig. 3(b)].

The sensitivity of xanthine in buffer, in FSV at 500 V s^{-1} (3.5 ± 0.4 μm radius), is 0.40 ± 0.02 nA μM^{-1} (0.995) in the concentration range of 0.5–6 μM and the LOD is 1.0 μM, based on the conservative estimate of S/N = 3. At 10 V s^{-1} the sensitivity is 0.038 nA μM^{-1}.[22] FSV of 400 nM xanthine shows resolved xanthine and uric acid peaks, although the S/N is low. The LOD for xanthine in FSV is similar to that in CE and HPLC. The speed of analysis is improved in FSV with the nanostructured sensor.

Xanthine and uric acid in xanthinuric and normal urine

In FSV measurements in 2000-fold diluted xanthinuric urine, the xanthine and uric acid oxidation peaks are well developed [Fig. 5(a)]. In 2000-fold diluted normal urine only the uric acid peak is observed [Fig. 5(b)]. The reverse reduction peaks are not well developed in urine samples.[25] Based on the known levels of xanthine in xanthinuric urine 2000-fold dilution was expected to result in ~1 μM concentration of xanthine in the diluted sample.

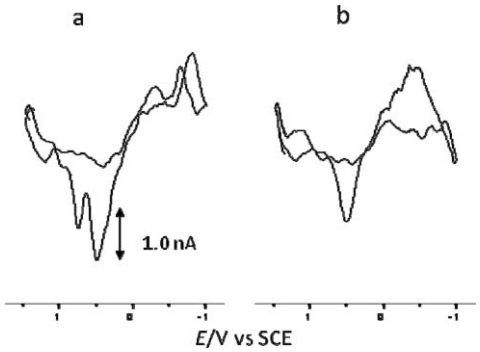

Fig. 5 Fast scan voltammetry in 2000-fold diluted urine: (a) xanthinuric and (b) normal; 500 V s^{-1}; 250 cycles averaged; background-subtracted with buffer background; sensor radius (a) 3.4 μm and (b) 3.1 μm.

The sensitivity of xanthine measurements in 2000-fold diluted xanthinuric urine by FSV at 500 V s^{-1} by standard addition is 0.80 ± 0.04 nA μM^{-1} (0.992); the xanthine concentration is 1.6 ± 0.2 μM or 3.2 ± 0.4 mM in the undiluted sample (Fig. 6). The concentration is near the 1 μM LOD of the method. Good signal-to-noise allows the measurements of xanthine concentrations in the vicinity of the LOD. From HPLC, the concentration of xanthine is 1.45 ± 0.07 μM or 2.90 ± 0.14 mM in the undiluted sample. The concentration of xanthine from HPLC and FSV is in agreement. From the standard addition, the concentration of uric acid in 2000-fold diluted normal urine is 3.80 ± 0.08 μM (0.99 nA μM^{-1}, 0.999) or 7.60 ± 0.16 mM in the undiluted urine, in agreement with the concentration determined by HPLC.

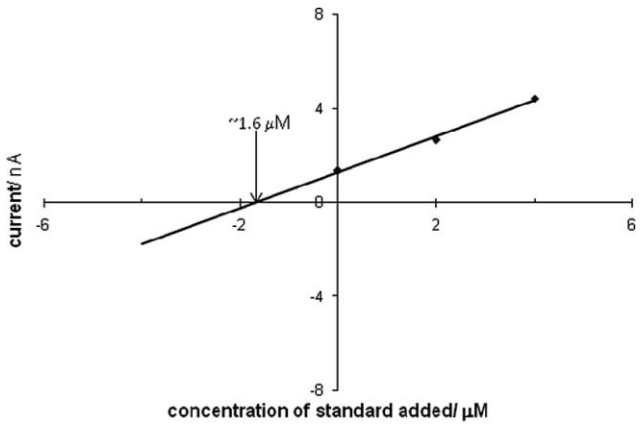

Fig. 6 Standard addition plot for xanthine concentration in 2000-fold diluted xanthinuric urine. Experimental conditions as in Fig. 5; sensor radius 3.4 μm.

Direct determinations of metabolite concentrations in urine

Advance calibration of the sensor in buffer speeds up the analysis compared to the standard addition method. For xanthine, the sensitivity in buffer is 0.40 ± 0.02 nA μM^{-1} (3.5 ± 0.4 μm radius) compared to 0.80 ± 0.04 nA μM^{-1} (3.5 ± 0.4 μm radius) from standard addition (Fig. 6). The higher sensitivity measured by standard addition is attributed to the lower and more stable background current in 2000-fold diluted urine at the oxidation peak potential of xanthine, compared to the background measured at the same potential in buffer [Fig. 2(c) and 5(a)]. Further investigations are necessary to understand the exact source of the higher sensitivity in xanthine measurements in the dilute urine samples, which are diluted with buffer. After the correction for the 2 : 1 sensitivity ratio, calibration curves obtained in buffer, before the measurements in urine samples, can be used to determine the xanthine concentration in the diluted urine samples. The sensitivity of uric acid is 0.99 ± 0.01 nA μM^{-1} (0.998) (3.5 ± 0.4 μm radius) in buffer in the concentration range of 0.5–4.5 μM and is the same as that from standard addition to urine samples.

The stability of the sensors was evaluated after the measurements of uric acid in the diluted urine sample, after the initial calibration of the sensor in buffer. For a 4 μM uric acid standard, the oxidation peak current was 3.91 ± 0.06 nA, before and after the measurements in urine samples (Fig. 7). A uric acid concentration of 3.95 ± 0.06 μM was determined from the calibration curve in buffer, in good agreement with the 4 μM concentration of the standard.

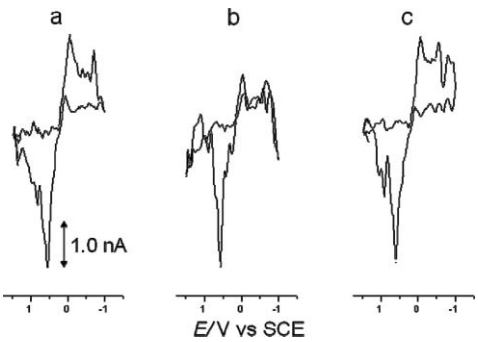

Fig. 7 Stability of the carbon fiber sensor in fast scan voltammetry measurements in urine: (a) 4 μM uric acid in buffer before the measurement in urine sample shown in (b); (b) sensor response in 2000-fold diluted normal urine after the measurement in (a); (c) 4 μM uric acid in buffer measured after the experiment in (b); experimental conditions as in Fig. 5; sensor radius 3.4 μm.

Conclusions

The high sensitivity of the nanostructured PAN carbon fiber sensors, with FSV as the signal acquisition method, was demonstrated in the measurements of two major purine metabolites – xanthine and uric acid – in highly diluted urine. For xanthine, high sensitivity is due to the low and stable background current at the sensor at the positive potentials of the xanthine oxidation peak. It appears that in the 2000-fold diluted urine samples, the sensor background is lowered, which stabilizes the background current. In addition, the high dilution of the

urine samples reduces matrix effects and reduces the interference from electroactive sample components in the measurements of xanthine and uric acid with the sensor.

The stability and reproducibility of fabrication of the sensors, which was verified from the measurements of sensor radius, and the electrochemical activity of the sensors in ferricyanide solution, allowed pooling of data from different analyses and for different sensors. The geometric disk radius of the sensors that were used for analysis of 3.5 ± 0.4 μm verified tight packing of the sealing resin and verified the absence of gaps in seals around the fiber.

The pathway of xanthine oxidation in FSV likely involves the initial $1e^-$ oxidation, which is followed by chemical reactions, and by $1e^-$ oxidation of the intermediates. High resolution of xanthine and uric acid peaks is achieved in FSV at 500 V s^{-1} at low concentrations of xanthine when the following chemical reactions do not distort the xanthine oxidation peak.

Xanthine and uric acid concentrations, determined with the nanostructured PAN carbon fiber sensor and FSV, and by HPLC, are in good agreement. Pre- or post-calibration of the sensor in buffer can be used in the determinations of xanthine and uric acid concentrations in urine to save time. The sensors are stable and can be used for repeated measurements. The method of determination of low concentrations of xanthine and uric acid that was developed will enable measurements of purine metabolites in cellular samples.

Acknowledgements

We would like to thank Dr Anne Simmonds (Purine Research Unit, Guy's Hospital, UK) and Dr Richard J. Johnson (Nephrology Department, University of Florida, USA) for the xanthinuric urine samples. We would also like to thank Dr Fatih Buyukserin and Dr Charles Martin (Department of Chemistry, University of Florida) for their help with SEM imaging. This work was partly funded by a grant from the Shands Hospital, Gainesville, FL through collaboration with Dr Richard J. Johnson.

References

1 G. la Marca, B. Casetta, S. Malvagia, E. Pasquini, M. Innocenti, M. A. Donati and E. Zammarchi, *J. Mass Spectrom.*, 2006, **41**, 1442.
2 E. S. Ford, C. Y. Li, S. Cook and H. K. Choi, *Circulation*, 2007, **115**, 2526.
3 I. Ben Zvi, Y. Green, F. Nakhoul, Y. Kanter and R. M. Nagler, *Nephron. Clin. Pract.*, 2007, **105**, 114.
4 A. A. Ejaz, W. Mu, D. H. Kang, C. Roncal, Y. Y. Sautin, G. Henderson, I. Tabah-Fisch, B. Keller, T. M. Beaver, T. Nakagawa and R. J. Johnson, *Clin. J. Am. Soc. Nephrol.*, 2007, **2**, 16.
5 E. Krishnan, C. K. Kwoh, H. R. Schumacher and L. Kuller, *Hypertension*, 2007, **49**, 298.
6 R. J. Johnson and B. A. Rideout, *New Engl. J. Med.*, 2004, **350**, 1071.
7 T. Kuhara, *J. Chromatogr., B*, 2002, **781**, 497.
8 T. Ito, A. B. P. van Kuilenburg, A. H. Bootsma, A. J. Haasnoot, A. van Cruchten, Y. Wada and A. H. van Gennip, *Clin. Chem. (Washington, D. C.)*, 2000, **46**, 445.
9 N. Cooper, R. Khosravan, C. Erdmann, J. Fiene and J. W. Lee, *J. Chromatogr., B*, 2006, **837**, 1.
10 C. Vidotto, D. Fousert, M. Akkermann, A. Griesmacher and M. M. Muller, *Clin. Chim. Acta*, 2003, **335**, 27.
11 R. Boulieu, C. Bory, P. Baltassat and C. Gonnet, *Anal. Biochem.*, 1983, **129**, 398.
12 L. Domanski, K. Safranow, M. Ostrowski, A. Pawlik, M. Olszewska, G. Dutkiewicz and K. Ciechanowski, *Arch. Med. Res.*, 2007, **38**, 240.
13 E. Causse, A. Pradelles, B. Dirat, A. Negre-Salvayre, R. Salvayre and F. Couderc, *Electrophoresis*, 2007, **28**, 381.
14 V. F. Samanidou, A. S. Metaxa and I. N. Papadoyannis, *J. Liq. Chromatogr. Relat. Technol.*, 2002, **25**, 43.
15 Q. C. Chu, M. Lin, C. H. Geng and J. N. Ye, *Chromatographia*, 2007, **65**, 179.
16 D. A. Mei, G. J. Gross and K. Nithipatikom, *Anal. Biochem.*, 1996, **238**, 34.
17 E. T. G. Cavalheiro and A. Brajter-Toth, *J. Pharm. Biomed. Anal.*, 1999, **19**, 217.
18 E. Palecek, *Anal. Biochem.*, 1980, **108**, 129.
19 J. L. Owens and G. Dryhurst, *Anal. Chim. Acta*, 1977, **89**, 93.
20 A. Brajter-Toth, K. Abou El-Nour, E. T. Cavalheiro and R. Bravo, *Anal. Chem.*, 2000, **72**, 1576.
21 A. D. Lazareck, S. G. Cloutier, T. F. Kuo, B. J. Taft, S. O. Kelley and J. M. Xu, *Nanotechnology*, 2006, **17**, 2661.
22 E. T. G. Cavalheiro, K. Abou El-Nour and A. Brajter-Toth, *J. Braz. Chem. Soc.*, 2000, **11**, 512.
23 B. E. K. Swamy and B. J. Venton, *Anal. Chem.*, 2007, **79**, 744.
24 R. Bravo, C. Hsueh, A. Jaramillo and A. Brajter-Toth, *Analyst*, 1998, **123**, 1625.
25 R. Bravo, D. M. Stickle and A. Brajter-Toth, *Methods in Molecular Biology*, Humana Press Inc., Totowa, New Jersey, 2002, ch. 21.
26 B. E. K. Swamy and B. J. Venton, *Analyst*, 2007, **132**, 876.
27 M. J. Logman, E. A. Budygin, R. R. Gainetdinov and R. M. Wightman, *J. Neurosci. Methods*, 2000, **95**, 95.
28 N. Arikyants, A. Sarkissian, A. Hesse, T. Eggermann, E. Leumann and B. Steinmann, *Pediatr. Nephrol.*, 2007, **22**, 310.
29 G. Rebentisch, S. Stolz and J. Muche, *Aktuel. Urol.*, 2004, **35**, 215.
30 F. A. Mateos, J. G. Puig, M. L. Jimenez and I. H. Fox, *J. Clin. Invest.*, 1987, **79**, 847.
31 T. Childers-Peterson and A. Brajter-Toth, *Anal. Chim. Acta*, 1987, **202**, 167.
32 C. Hsueh, R. Bravo, A. J. Jaramillo and A. Brajter-Toth, *Anal. Chim. Acta*, 1997, **349**, 67.
33 M. Vonstackelberg, M. Pilgram and V. Toome, *Z. Elektrochem.*, 1953, **57**, 342.
34 P. Tschuncky and J. Heinze, *Anal. Chem.*, 1995, **67**, 4020.
35 C. Ronco and F. Rodeghiero, *Hyperuricemic Syndromes: Pathophysiology and Therapy*, Karger, New York, 2005, vol. 147, p. 72.
36 J. X. Feng, M. Brazell, K. Renner, R. Kasser and R. N. Adams, *Anal. Chem.*, 1987, **59**, 1863.
37 J. B. Donnet and R. C. Bansal, *Carbon Fibers*, Marcel Dekker, New York, 2nd edn, 1990.
38 C. A. Goss, J. C. Brumfield, E. A. Irene and R. W. Murray, *Anal. Chem.*, 1993, **65**, 1378.
39 J. C. O'Brien, J. Shumaker-Parry and R. C. Engstrom, *Anal. Chem.*, 1998, **70**, 1307.
40 M. G. Sullivan, B. Schnyder, M. Bartsch, D. Alliata, C. Barbero, R. Imhof and R. Kotz, *J. Electrochem. Soc.*, 2000, **147**, 2636.
41 N. Oya and D. J. Johnson, *Carbon*, 2001, **39**, 635.
42 M. X. Ji, C. G. Wang, Y. J. Bai, M. J. Yu and Y. X. Wang, *Polym. Bull.*, 2007, **59**, 527.
43 C. Kim, S. H. Park, J. K. Cho, D. Y. Lee, T. J. Park, W. J. Lee and K. S. Yang, *J. Raman Spectrosc.*, 2004, **35**, 928.
44 M. L. A. V. Heien, P. E. M. Phillips, G. D. Stuber, A. T. Seipel and R. M. Wightman, *Analyst*, 2003, **128**, 1413.
45 R. Bravo and A. Brajter-Toth, *Anal. Chem. (Warsaw)*, 1999, **44**, 423.
46 A. J. Bard and L. R. Faulkner, *Electrochemical Methods, Fundamentals and Applications*, Wiley, New York, 1980.
47 J. L. Owens, H. A. Marsh and G. Dryhurst, *J. Electroanal. Chem.*, 1978, **91**, 231.
48 A. J. S. C. Vieira and S. Steenken, *J. Chim. Phys.*, 1996, **93**, 235.
49 A. J. S. C. Vieira, J. P. Telo and R. M. B. Dias, *J. Chim. Phys.*, 1997, **94**, 318.
50 J. Santamaria, C. Pasquier, C. Ferradini and J. Pucheault, *Radiat. Res.*, 1984, **97**, 452.
51 G. Dryhurst, *J. Electrochem. Soc.*, 1972, **119**, 1659.
52 S. V. Jovanovic and M. G. Simic, *J. Phys. Chem.*, 1986, **90**, 974.
53 K. N. Rogstad, Y. H. Jang, L. C. Sowers and W. A. Goddard, *Chem. Res. Toxicol.*, 2003, **16**, 1455.
54 C. C. Hsueh and A. Brajter-Toth, *Anal. Chem.*, 1993, **65**, 1570.

